CHEMISTRY OF MATERIALS

pubs.acs.org/cm Article

Flexibility of a Metal–Organic Framework Enhances Gas Separation and Enables Quantum Sieving

Omid T. Qazvini, Victoria-Jayne Scott, Linda Bondorf, Maxime Ducamp, Michael Hirscher, François-Xavier Coudert, and Shane G. Telfer*

Cite This: *Chem. Mater.* 2021, 33, 8886–8894 Read Online

ACCESS | Metrics & More | Article Recommendations | Supporting Information

ABSTRACT: Flexible metal–organic frameworks (MOFs) undergo reversible structural transformations triggered by external stimuli. An interesting feature of some MOFs is their ability to flex in response to specific guests, which can enable selective separation. Here, we introduce MUF-15-OMe ($[Co_6(\mu_3\text{-}OH)_2(ipa\text{-}OMe)_5(H_2O)_4]$), a variant of MUF-15 that comprises hexanuclear cobalt(II) clusters connected by 5-methoxyisophthalate (ipa-OMe) ligands. MUF-15 itself has isophthalate linkers and is inflexible upon uptake of common gases. On the other hand, MUF-15-OMe flexes upon the uptake of gases such as CO_2 and C_2 hydrocarbons at pressures less than 1 bar, as revealed by distinct steps in its gas adsorption isotherms. Computational analysis showed that the underlying mechanism involves partial detachment of one of the carboxyl groups of the framework linkers. The gas pressure required to induce framework dynamics can be tuned by replacing some of the ipa-OMe by isophthalate ligands in multivariate frameworks. The flexing of MUF-15-OMe opens up space for the adsorption of specific additional gas molecules. This enhances the separation of CO_2 and N_2 and enables the differentiation of H_2 and D_2 by quantum sieving. By providing a clear illustration of how flexibility allows the discrimination of gas mixtures, this study underpins the use of dynamic MOFs for challenging separations.

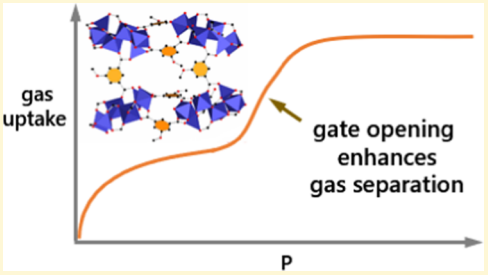

INTRODUCTION

Metal–organic frameworks (MOFs) benefit from atomic-level precision coupled to rich structure–property relationships.[1,2] While most frameworks are rigid with unvarying structures,[3,4] certain frameworks are dynamic and respond to external stimuli.[5−8] When a MOF flexes, the structural deformation can originate from (a) motion of the organic ligands, (b) distortion of the metal–ligand interactions, (c) the arrangement of ions with metal clusters, and/or (d) the movement of interpenetrated subnets. Combinations of these effects are common. The connectivity between the components is typically maintained when dynamic MOFs flex, which maintains the integrity of the framework and means that the dynamic process is reversible.[6,9,10] The adsorption of gas molecules is a well-investigated way of stimulating structural transformations in MOFs. A dense MOF can be pried open above a certain threshold pressure or, alternatively, the framework may be porous both before and after the transformation.[11,12] Since the framework is porous prior to the flexing in this latter case, the adsorption isotherm exhibits two distinct steps.

Dynamic processes in MOFs can be influenced by functional groups on the linkers.[13−18] For example, certain moieties on the bdc ligand in MIL-53 can tune the gas pressure at which the narrow pore form is converted into the large pore form.[17] A fine balance is struck between the stability of large and narrow pore forms and the guest–framework interactions. The narrow pore form is inherently more stable than the large pore form due to hydrogen bonds. However, when guests are admitted into the framework, favorable noncovalent interactions induce pore opening.

Dynamic MOFs are attractive for gas separations since flexing can enhance host–guest interactions to improve their uptake capacity and boost their selectivity.[19−26] We previously reported MUF-15, $[Co_6(\mu_3\text{-}OH)_2(ipa)_5(H_2O)_2]$, which comprises hexanuclear cobalt(II) clusters and isophthalate (ipa) linkers.[27] The hydrogen atom at the 5-position of the phenyl ring in MUF-15 is positioned toward a framework cavity, which allows functional groups (−F, −OH, −Br, $-NO_2$, and $-CH_3$) to be introduced via 5-substituted isophthalic acid linkers.[28] While we observed hints of framework flexibility in these materials, their overall dynamic behavior was subtle. We now report on a material with pronounced dynamic transformations: a methoxy derivative of MUF-15 derived from 5-methoxylisophthalate (MUF-15-OMe). Computational analysis illustrates the flexing process at the molecular level, and the additional space upon gate opening enhances the separation of CO_2 and N_2 and enables the differentiation of H_2 and D_2 by quantum sieving.

Received: September 15, 2021
Revised: October 18, 2021
Published: November 2, 2021

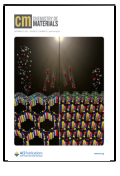

https://doi.org/10.1021/acs.chemmater.1c03170
Chem. Mater. 2021, 33, 8886–8894

EXPERIMENTAL SECTION

Synthesis of MUF-15-OMe. A mixture of $Co(OAc)_2{\cdot}4H_2O$ (0.125 g, 0.5 mmol), 5-methoxyisophthalic acid (0.171 g, 0.875 mmol), MeOH (7 mL), and H_2O (0.5 mL) was sonicated for 10 min and then sealed in a 25 mL Teflon-lined autoclave and heated to 120 °C for 48 h. After cooling to room temperature, the resulting purple crystals were washed with methanol several times and dried under vacuum. The yield was ca. 0.098 g, 82% (based on cobalt acetate). Guest-free MUF-15-OMe was produced by placing the crystals under vacuum overnight at 120 °C.

MUF-15-OMe Doped with Isophthalic Acid. A mixture of $Co(OAc)_2{\cdot}4H_2O$ (0.125 g, 0.5 mmol), 5-methoxyisophthalic acid, isophthalic acid, MeOH (6 mL), and H_2O (0.5 mL) was sonicated for 20 min and sealed in a 25 mL Teflon-lined autoclave and heated to 140 °C for 48 h. After cooling to room temperature, the resulting purple crystals were washed with methanol several times and dried under vacuum. Ligand ratios were determined by ^1H nuclear magnetic resonance (NMR) spectroscopy on dissolved samples. $[Co_6(\mu_3\text{-}OH)_2(ipa)_{0.59}(ipa\text{-}OMe)_{4.41}(H_2O)_4]$, (88.3% ipa-OMe, 11.7% ipa): synthesized using 5-methoxyisophthalic acid (0.156 g, 0.80 mmol) and isophthalic acid (0.33 g, 0.20 mmol). $[Co_6(\mu_3\text{-}OH)_2(ipa)_{0.32}(ipa\text{-}OMe)_{4.68}(H_2O)_4]$, (93.5% ipa-OMe, 6.5% ipa): synthesized using 5-methoxyisophthalic acid (0.177 g, 0.90 mmol) and isophthalic acid (0.16 g, 0.10 mmol).

X-ray Diffraction. As-synthesized samples were washed several times with methanol before being mounted on the instrument. All PXRD data for pure MUF-15-OMe were collected at room temperature on a Rigaku Spider diffractometer equipped with a MicroMax MM007 rotating anode generator (Cu α radiation, 1.54180 Å), high-flux Osmic multilayer mirror optics, and a curved image plate detector. For aging experiments on activated frameworks, after washing the as-synthesized samples several times with MeOH, they were activated and exposed to air with a high relative humidity (~70%) at 20 °C.

The SCXRD data for MUF-15-OMe and unit cell and PXRD data for doped materials were collected at room temperature on a Bruker Venture D8 diffractometer equipped with a IμS DIAMOND source (Cu α radiation, 1.54178 Å) and a Photon III detector. Crystals of MUF-15-OMe diffracted poorly, and the best results were obtained at room temperature. As a consequence, the SCXRD data were truncated at 0.90 Å during the refinement. All atoms were allowed to freely refine during the refinement except those of the occluded water molecules, which were found on the difference map then held in fixed positions.

Low-Temperature Thermal Desorption Spectroscopy. The sample was cooled to the exposure temperature under vacuum and then exposed to the gas atmosphere for the exposure time. After a 1 min evacuation under high vacuum, the MOF was further cooled to 20 K and heated to 300 K at a constant heating rate of 0.1 K/s. During the heating, mass spectral data, gas pressure as a function of time, are collected to determine the rate of desorption of each gas. Quantitative uptake and selectivity values can be calculated. For this purpose, the calibration alloy $Pd_{95}Ce_5$ was placed under a hydrogen or deuterium atmosphere at 16 mbar and 353 K for 2 h. Before and after absorption, the alloy was weighed to determine the amount of gas loaded. The alloy sample was then heated to 600 K at 0.1 K/s for desorption. The integral of the desorption pressure over time corresponds to the amount of desorbed gas molecules and thus to the weight-determined gas loading. The ratio of the measured change in weight to the determined amount of gas through the desorption integral was used as a specific calibration constant.

RESULTS AND DISCUSSION

The solvothermal reaction of cobalt acetate and 5-methoxyisophthalic acid (H_2ipa-OMe) yields violet platelike single crystals of MUF-15-OMe, $[Co_6(\mu_3\text{-}OH)_2(ipa\text{-}OMe)_5(H_2O)_4]$. MUF-15-OMe crystalizes in the $P2_12_12$ space group. Although this space group differs from that seen for MUF-15 (*Pnna*), their unit cell volumes are similar (Table 1). The phase purity of the framework activated at 120 °C was confirmed by matching its powder X-ray diffraction (PXRD) pattern with that simulated from its single-crystal X-ray diffraction (SCXRD) structure (Figures S6−S8).

Table 1. Calculated and Experimentally Determined Structural Parameters of MUF-15 and MUF-15-OMe[a,b]

MOF	MUF-15	MUF-15-OMe[a,c]
unit cell volume (Å^3)	6640	7082
Brunauer−Emmett−Teller (BET) surface area[b,c] (m^2/g)	1130	837
calculated surface area[c] (m^2/g)	1207	999
experimental pore volume[b,c] (cm^3/g)	0.51	0.36
calculated pore volume[c] (cm^3/g)	0.46	0.38
PLD/LCD (Å)[c,d]	3.6/5.2	3.4/5.0

[a]Prior to gate opening. [b]From the N_2 adsorption isotherm at 77 K. [c]Calculated using RASPA and Zeo++. [d]PLD: pore limiting diameter. LCD: largest cavity diameter.

MUF-15-OMe comprises hexanuclear clusters that are built up from two symmetry-related sets of cobalt(II) ions (Figure 1a). The 5-methoxyisopthalate (ipa-OMe) linkers further assemble the clusters into a porous 3D network (Figure 1b−d). Each cluster coordinates to 10 ipa-OMe linkers in total, with eight linkers connecting adjacent clusters in the (*bc*) plane. Two additional linkers are oriented along the crystallographic *a* direction. These linkers are orthogonal to the main plane of the clusters, and they connect each cluster to a partner above or below it (Figure 1c). The disposition of these axial linkers subtly depends on the functional group at the 5-position of the isophthalate ligand. Hydrogen and fluoro substituents lead to a zig-zag orientation, while methyl and bromo groups lead to titling in the same direction (Figure S5). A third arrangement is evident in MUF-15-OMe (Figure 1c). Here, the ligands tilt in an alternating, zig-zag fashion along the *a* direction. MUF-15-OMe is thus a topological isomer of MUF-15 rather than being strictly isoreticular with it.

MUF-15-OMe is thermally and hydrolytically stable, which allows for easy handling. Thermogravimetric analysis (TGA) shows a mass loss of 10−20% up to 100 °C, corresponding to the escape of occluded guest water molecules, and the guest-free framework is stable up to 300 °C (Figure S10) and under humid atmospheres (Figure S6). In comparison, MUF-15 is stable in air for only a week and loses crystallinity over that time. To quantify the stability of MUF-15-OMe toward humid air, we measured gas adsorption isotherms before and after exposure to ambient air. The uptake of CO_2 by aged MUF-15-OMe is 60.2 cm^3/g (at 1 bar), which is almost identical to a pristine sample (60.6 cm^3/g) (Figure S12).

A N_2 adsorption isotherm of MUF-15-OMe was recorded at 77 K (Figure S18). Its BET surface area is 837 m^2/g, and its total pore volume is 0.36 cm^3/g (Table 1 and Figure S18). These values are close to the geometric surface area (999 m^2/g) and pore volume (0.38 cm^3/g) calculated from the crystallographic coordinates (Table 1). As expected, the introduction of the methoxy functional group reduces the pore volume and surface area of MUF-15-OMe in comparison to the parent MUF-15. This decrease can be explained by the occupation of void space by the methoxy groups, but we note that this is counteracted in part by the greater unit cell volume of MUF-15-OMe compared to MUF-15. Connolly surfaces with a probe of 1 Å were plotted for MUF-15-OMe (Figure 1d) and MUF-15 (Figure S2) to compare their pore architectures. There are significant channels along the crystallographic *c* direction (~3.5 × 6.0 Å^2) in MUF-

https://doi.org/10.1021/acs.chemmater.1c03170
Chem. Mater. 2021, 33, 8886−8894

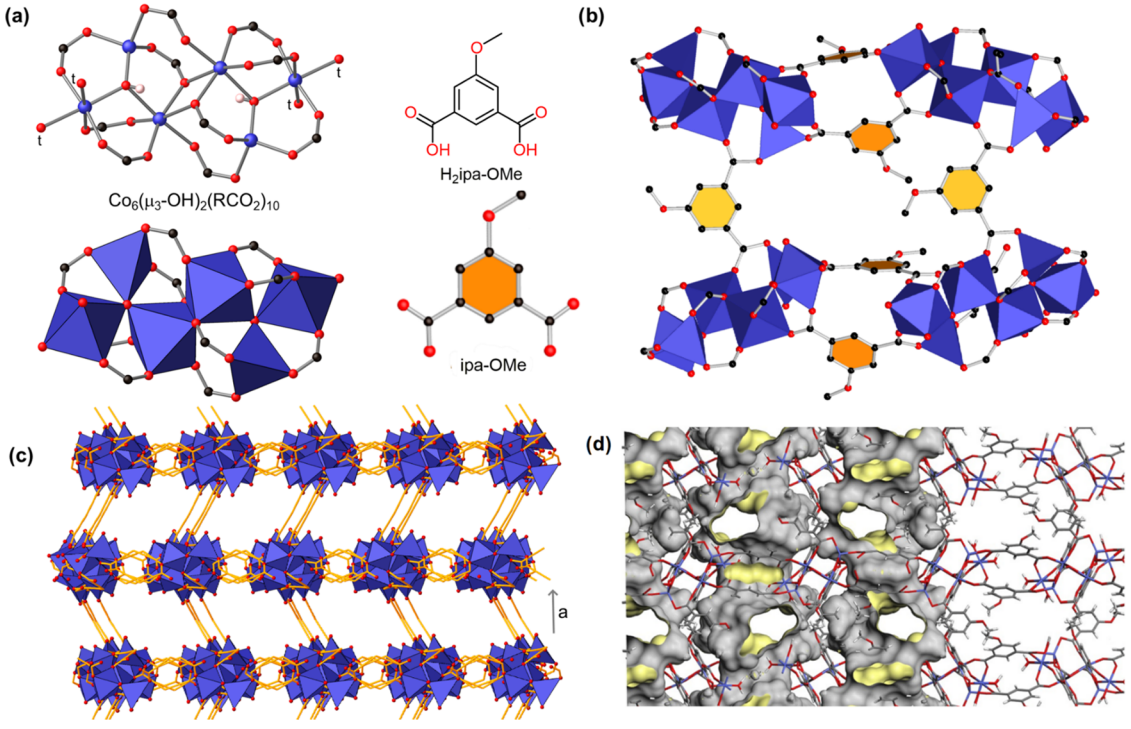

Figure 1. (a) SCXRD structure of MUF-15-OMe comprises hexanuclear cobalt(II) clusters (cobalt = dark blue; oxygen = red; carbon = gray; hydrogen = pale pink (mostly omitted for clarity)) connected by 5-methoxyisophthalate (ipa-OMe) linkers. Sites occupied by terminal H_2O ligands are marked with the letter t. (b, c) Cobalt(II) clusters and ipa-OMe ligands assemble into a network that defines a 3D array of channels in MUF-15-OMe. Each cluster is connected to 10 others by bridging ipa-OMe ligands. (d) Network of pores in MUF-15-OMe illustrated by the Connolly surface in yellow (probe of diameter 1.0 Å). The outer surface of the pore space network is shown in gray.

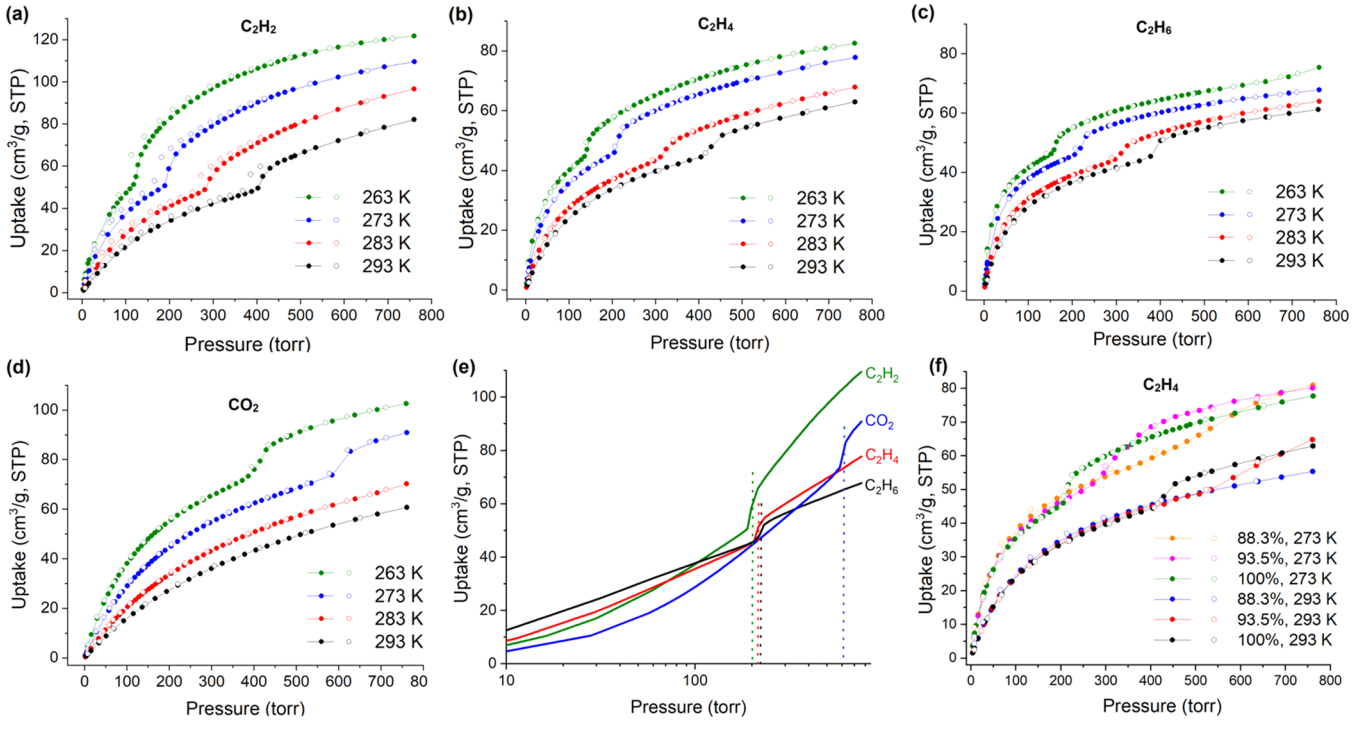

Figure 2. Volumetric (a) C_2H_2, (b) C_2H_4, (c) C_2H_6, and (d) CO_2 adsorption (filled circles) and desorption (open circles) isotherms measured at different temperatures for MUF-15-OMe. (e) Volumetric adsorption isotherms measured at 273 K for MUF-15-OMe presented using a log scale on the *x*-axis. The vertical dashed lines indicate the gate opening pressure of each gas. (f) Volumetric C_2H_4 adsorption (filled circles) and desorption (open circles) isotherms measured at 273 and 293 K for $[Co_6(\mu_3\text{-}OH)_2(ipa)_{0.32}(ipa\text{-}OMe)_{4.68}(H_2O)_2]$ (93.5% ipa-OMe) and $[Co_6(\mu_3\text{-}OH)_2(ipa)_{0.59}(ipa\text{-}OMe)_{4.42}(H_2O)_2]$ (88.3% ipa-OMe). The percentages represent how much ipa-OMe is present as a fraction of the total isophthalate content.

https://doi.org/10.1021/acs.chemmater.1c03170
Chem. Mater. 2021, 33, 8886−8894

15-OMe and smaller, more tortuous channels in the crystallographic *a* direction. The PXRD pattern of MUF-15-OMe changes slightly when the occluded solvent is removed under vacuum (Figure S8). The diffraction peak at $2\theta = 7.5°$ disappears under vacuum, and the peaks at 2θ = 8.0 and 9.0° move to a higher angle. The diffraction pattern reverts to that of the as-synthesized state after exposing the evacuated sample to the atmosphere. These changes are consistent with reversible flexing of the framework.

The dynamic behavior of MUF-15-OMe was substantiated by measuring low-pressure gas adsorption isotherms with C_2H_6, C_2H_4, C_2H_2, and CO_2 at a range of temperatures (Figure 2). Stepped isotherms were observed in all cases, except for the uptake of CO_2 at 283 and 293 K, where the step is likely to exist at above 1 bar. Taking the C_2H_2 adsorption isotherms as an example (Figure 2a), the uptake at 263 K proceeds steadily at low pressures in a Langmuir-like fashion. At a pressure of 110 Torr, there is then a sharp jump in gas uptake from 50 to 70 cm^3/g. This indicates flexing of the framework, which creates additional framework space to allow an increase in C_2H_2 adsorption. At 293 K, the C_2H_2 pressure for the second adsorption step increases from 100 to ~400 Torr, while the amount of adsorbed gas required to induce flexing is fairly constant (51 cm^3/g at 263 K; 46 cm^3/g at 293 K). Similar trends are observed for the adsorption of C_2H_4 and C_2H_6 (Figure 2b,c). Gate opening is also evident at low temperatures; in the CO_2 and C_2H_4 adsorption isotherms at 195 K (Figures S13 and S14), we observed the isotherm steps at pressures of 1 and 85 Torr, respectively, with uptakes of 40 and 130 cm^3/g. Lower temperatures increase the gas loading and therefore a lower pressure is required for the structural transition. The gate opening pressure of MUF-15-OMe is sensitive to the adsorbate, with C_2H_2 being the most effective at prying open the framework (Figure 2e). C_3H_8 and C_3H_6 isotherms exhibit no distinct jumps (Figure S15). We speculate that these gases may induce framework gate opening behavior at very low pressures so the first and second adsorption steps are indistinguishable.

The parent MUF-15 material is built up from isophthalic acid (H_2ipa).[27] MUF-15 isotherms have standard Langmuir shapes and do not exhibit flexibility below 1 bar. We thus reasoned that the flexibility of MUF-15-OMe could be tuned by doping with isophthalate (ipa) linkers. To this end, we synthesized multivariate frameworks with variable levels of included ipa: $[Co_6(\mu_3\text{-}OH)_2(ipa)_{0.59}(ipa\text{-}OMe)_{4.42}(H_2O)_2]$ (88.3% ipa-OMe) and $[Co_6(\mu_3\text{-}OH)_2(ipa)_{0.32}(ipa\text{-}OMe)_{4.68}(H_2O)_2]$ (93.5% ipa-OMe). ^{1}H NMR spectroscopy was used to quantify the ligand ratios (Figures S26 and S27). PXRD and unit cell determinations indicate that the MUF-15-OMe framework structure is preserved upon the inclusion of ipa ligands (Figure S7 and Tables S2 and S3). As anticipated, the inclusion of ipa linkers increases the gate opening pressure and the sharpness of the second adsorption step decreases with increasing ipa content (Figures 2f and S16). A shift in the gate opening pressure also occurs for CO_2 (Figure S17); however, a distinct step is only observed below 1 bar at 273 K. The inclusion of ipa linkers tunes the gate opening pressure by counteracting the framework flexing.

The isosteric heats of adsorption (Q_{st})[29] calculated at low uptake show that MUF-15-OMe has a high affinity for C_2H_2 (31.4 kJ/mol), followed by C_2H_4, C_2H_6, and CO_2 (29.4, 27.9, and 26.9 kJ/mol, respectively, Figure S20). This trend indicates that stronger MOF−guest interactions result in lower gate opening pressures.

To understand the structural details of the flexing process, we performed ab initio simulations on MUF-15-OMe and its parent structure, MUF-15, at the quantum chemical level. We followed a methodology previously used in exploring the flexibility of novel (or hypothetical) compounds.[30] The lower symmetry, large dimensionality, and the presence of very soft degrees of freedom in MUF-15-OMe prevented calculations from converging within the high accuracy required. We therefore performed the computational analysis on the parent MUF-15 compound in the *Pnna* space group (Figure 3a).

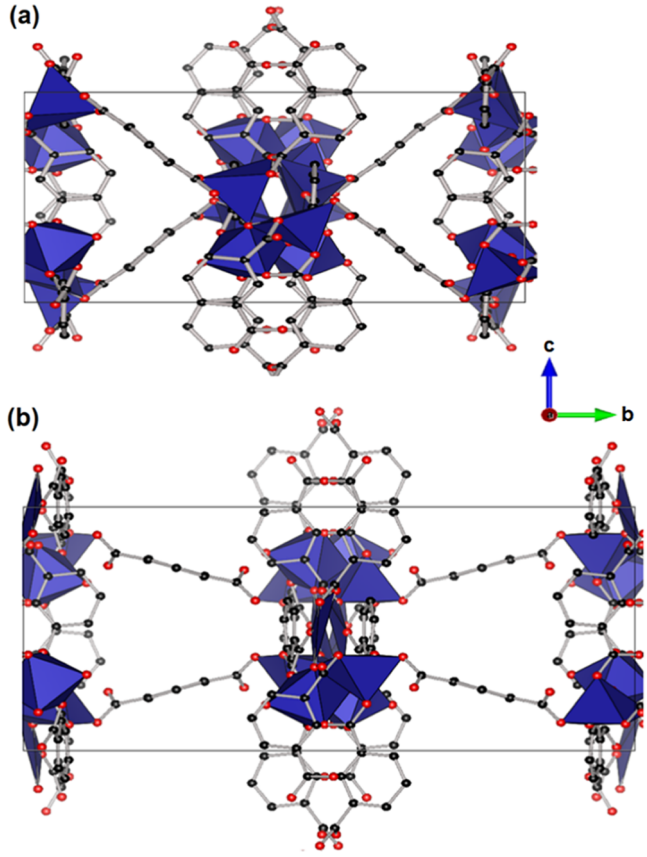

Figure 3. (a) Structure of parent MUF-15, $[Co_6(\mu_3\text{-}OH)_2(ipa)_{10}]$, at equilibrium, from DFT calculations. (b) Structure of parent MUF-15, $[Co_6(\mu_3\text{-}OH)_2(ipa)_{10}]$, after an increase of volume of ΔV = +32% due to detachment of one of the ipa linkers from the cobalt cluster.

We first gradually applied an isotropic negative pressure on the structure to simulate framework opening under a guest-induced adsorption stress.[31] In response, we observed a small variation of the *a* and *c* parameters of around 0.3 Å (over the range of 0 to −1.6 GPa), while the *b* parameter varied more significantly—around 2.3 Å. This demonstrates the potential for flexibility in the MUF-15 family and highlights an important anisotropy in the microscopic mechanism, with the *b* direction being by far the softest. At an applied pressure of −1.7 GPa, an even more pronounced increase was seen in the *b* cell parameter of >1.3 Å over 0.1 GPa. Here, one of the ipa linkers, aligned along *b*, detaches from the cobalt cluster (Figure 3b).

To further investigate the variation of the cell parameters around the pressure of interest, we performed a series of constant-volume minimizations (where atomic positions and cell parameters are optimized with only a constraint on total volume). The structures obtained (available as the Supporting

https://doi.org/10.1021/acs.chemmater.1c03170
Chem. Mater. 2021, 33, 8886−8894

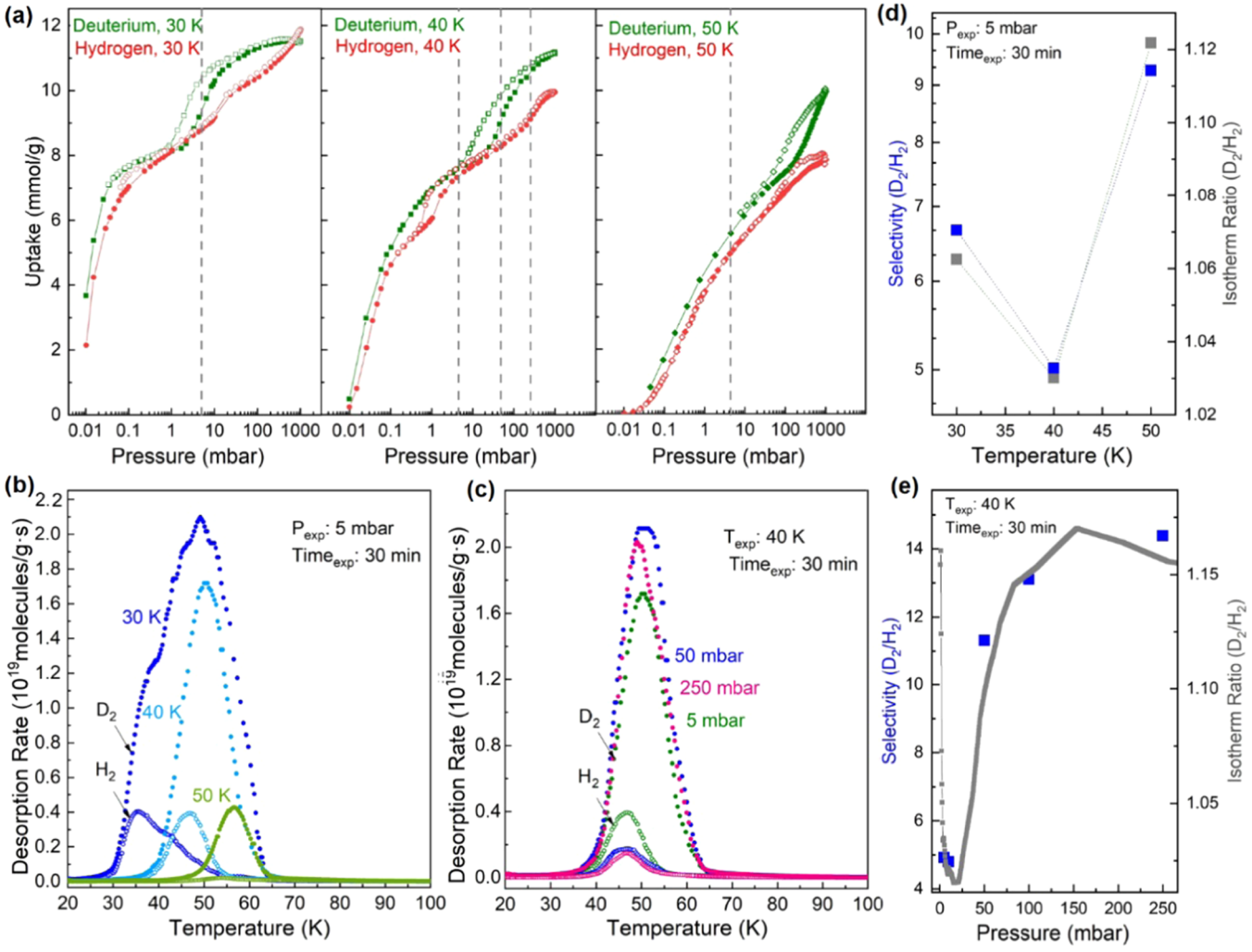

Figure 4. (a) Semilogarithmic representation of MUF-15-OMe isotherms for H_2 and D_2 at 30, 40, and 50 K. The gray lines indicate the conditions at which TDS measurements with a 1:1 isotope mixture were performed. (b) Desorption of MUF-15-OMe for 30, 40, and 50 K exposure temperature: TDS desorption rate at 5 mbar exposure pressure and 30 min exposure time. (c) Desorption of MUF-15-OMe for 5, 50, and 250 mbar exposure pressure: TDS desorption rate at 40 K exposure temperature and 30 min exposure time. Selectivity determined by TDS and the isotope ratio of MUF-15-OMe as a function of exposure temperature (d) and of exposure pressure (e). The isotherm ratio was determined for 52 pressure points; TDS measurements were carried out at four different pressures.

Information) confirm the microscopic mechanism: first, as the volume increases, the linkers orient in the *b* direction and flatten in the *ab* plane. This is followed by cleavage of one of the Co−O coordination bonds aligned in the *b* direction. This explains the strong anisotropy of the mechanical properties.

To ascertain the impact of this flexibility on the pore network, we calculated the surface area and accessible volume of both structures with Zeo++. The parent structure has a surface area of 1391 m^2/g and an accessible volume of 0.079 cm^3/g. These values are lower than those derived from the experimental structure, which is consistent with the smaller unit cell volume of the energy-minimized structure. Upon increasing the unit cell volume from 5807 to 7648 $Å^3$, the values for the surface area and accessible volume jumped to 2357 m^2/g and 0.260 cm^3/g, respectively. Framework flexibility is clearly associated with a drastic change to the pore network, demonstrating how it can be coupled to (and triggered by) the adsorption of guest molecules with significant host−guest interaction strengths.

We confirmed the accessibility of this open phase by calculating the energy penalty for the opening process. As our simulations are performed on the neat framework, the denser phase is expected to be more stable. The energy difference is E = +54 kJ/mol per Co atom. This is comparable to "breathing" energies observed for other porous MOFs and fully consistent with materials where flexibility can be triggered by adsorption. We also confirmed that the structure in Figure 3b corresponds to a metastable phase, being a local minimum of the enthalpy ($H = U + PV$). The mechanism observed for MUF-15 appears to be generic, although the details of the energetic balance involved in the opening process will depend on the microscopic nature of each structure: this means that while we expect all members of the MUF-15 family to have the potential to be flexible, flexing will be triggered under different conditions (temperature, pressure, adsorption) in different materials. This is in line with the experimental observations.

With an eye to exploiting the flexibility of MUF-15-OMe for quantum sieving, we measured adsorption isotherms of H_2 and D_2 at 30−50 K (Figure 4a). These isotherms exhibit stepwise and hysteretic adsorption, which are both indicators of structural flexibility. At their boiling temperatures, the framework opening pressures of H_2 (0.07 mbar) and D_2 (0.04 mbar) differ slightly (Figure S28). At higher temperatures, gate opening is

https://doi.org/10.1021/acs.chemmater.1c03170
Chem. Mater. 2021, 33, 8886−8894

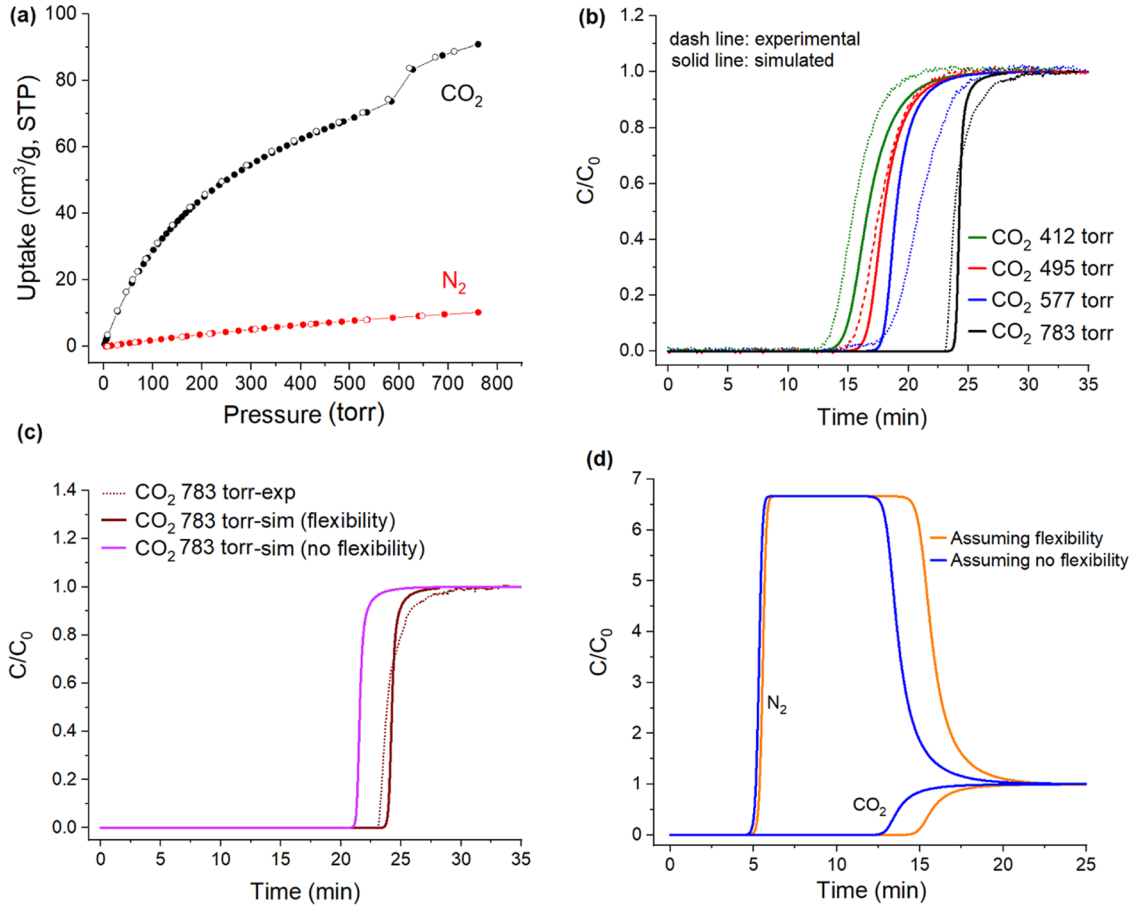

Figure 5. (a) Volumetric CO_2 and N_2 adsorption (filled circles) and desorption (open circles) isotherms measured at 273 K for MUF-15-OMe. (b) Experimental and predicted single-component breakthrough curves of CO_2 in a column packed with MUF-15-OMe with a total pressure of 1.1 bar. (c) Predicted single-gas breakthrough curves for CO_2 at 0.95 bar assuming MUF-15-OMe to be either rigid (pink) or flexible (brown). (d) Predicted breakthrough curve for an 85/15 CO_2/N_2 mixture for a bed packed with MUF-15-OMe at 273 K and 1.1 bar assuming the framework to be either rigid (blue) or flexible (orange).

consistently induced at lower pressure by D_2 compared to H_2. At 30 and 40 K, the difference in opening pressure is more than 1 order of magnitude, which is comparable to results reported for the breathing MOF MIL-53(Al) at 77 K.[32] In accord with the earlier-reported gases, the position of a gate opening for H_2 and D_2 shifts toward higher pressures with increasing temperature. A similar shift in the gate opening pressure has been reported for high-pressure H_2 adsorption in Co(1,4-benzendipyrazolate)[33] and for cryogenic low-pressure adsorption in MIL-53(Al).[32]

Hydrogen isotope separation is a key technological challenge in the development of hydrogen fuel systems, chemical reaction mechanism labeling, neutron scattering techniques, pharmaceutical technology, nonradioactive isotopic tracing, lighting, etc.[34−38] Invigorated by significant differences in the single-component adsorption isotherms of H_2 and D_2, we investigated MUF-15-OMe for this separation.

The ability of a material to be used for isotope separation can be analyzed indirectly via its pure gas isotherms or directly by thermal desorption spectroscopy (TDS)[39] of a 50/50 gas mixture (Figure 4b,c). The molar isotherm ratio D_2/H_2 as a function of temperature and pressure, as well as the selectivity determined by TDS measurements with a 50/50 mixture of the isotopes, is displayed in Figure 4d,e. Here, temperature and pressure refer to the gas exposure conditions, which are indicated by gray lines in the corresponding isotherm (Figure 4a). Both selectivity and the isotherm ratio decrease as a function of temperature from 30 to 40 K, followed by a steep increase to 50 K. The selectivity decreases from 6.3 at 30 K to 4.9 at 40 K. It increases strongly to 9.8 at 50 K. With increasing pressure at 40 K, the molar ratio first drops at low pressures below 20 mbar, followed by a rapid increase from a minimum of 1.02 to a maximum of 1.17 at 140 mbar. The selectivity of MUF-15-OMe follows this trend with a drop between 5 and 10 mbar, a significant selectivity increase to 50 mbar and a more gradual increase to 100 and 250 mbar. The highest selectivity value of 14.3 for MUF-15-OMe was measured at 40 K and 250 mbar. This can be compared with other highly selective materials such as CPO-27[37] (11.8 at 60 K and 30 mbar), MIL-53(Al)[32] (13.6 at 40 K and 10 mbar), and FMOFCU[38] (14 at 25 K and 10 mbar). MUF-15-OMe outperforms these materials when selectivity and uptake capacity are considered together. In the breathing region at 40 K and pressures between 50 and 250 mbar (kinetic quantum sieving mechanism), we observe a selectivity of 14.3 and uptake of 4.75 mmol/g for MUF-15-OMe, which is higher than CPO-27[37] (selectivity of 11.8 and uptake below 3 mmol/g at 60 K and 30 mbar), MIL-53(Al)[32] (selectivity of 13.6 and uptake of 2 mmol/g at 40 K and 10 mbar, and for higher pressure 80 mbar, the uptake increases to 8 mmol/g, but the selectivity drops to 6), and FMOFCU[38] (selectivity of 14 and uptake of 0.1 mmol/g at 25 K and 10 mbar).

The pressure-dependent selectivity, measured by TDS at 40 K, spans the pressure ranges 5−10 mbar, prior to the D_2

https://doi.org/10.1021/acs.chemmater.1c03170
Chem. Mater. 2021, 33, 8886−8894

adsorption step, and the range 50−250 mbar, where the framework flexes (Figure 4a,c). The rapid increase in the total uptake between 10 and 50 mbar arises from the additional pore space generated by gate opening (Figure S29b). The significant increase in selectivity over this pressure range indicates that the kinetic quantum sieving is enabled by the flexing of MUF-15-OMe since D_2 diffuses faster than H_2 in the newly created void space (Figure 4e).

Temperature-dependent selectivity measurements align with this finding (Figure 4d). At 40 K, 5 mbar lies below the adsorption step, while at 30 K, this pressure falls inside the hysteresis zone. The selectivity of MUF-15-OMe at 5 mbar decreases from 30 to 40 K. This is due to the adsorption-driven opening of the additional pore at 30 K, which enables kinetic quantum sieving. In contrast, at 5 mbar and 40 K, the additional pores are still closed, so they have no beneficial impact on selectivity. The high selectivity at 50 K and 5 mbar could originate from chemical affinity sieving. Due to evacuation at the exposure temperature, only strongly bound molecules remain at the surface, which leads to a decrease in total uptake with increasing exposure temperature. Moreover, at stronger adsorption sites, there is a preference for D_2 adsorption, resulting in a higher selectivity by chemical affinity quantum sieving.

We then turned to the separation of CO_2 and N_2. The effect of MOF flexibility on chemical separations is a topical research field.[19,40−42] We made measurements at 273 K due to the favorable isotherm profiles at this temperature: the low-pressure CO_2 isotherm of MUF-15-OMe features the second adsorption step around 620 Torr, while the N_2 isotherm does not have a second adsorption step (Figure 5a). We therefore reasoned that enhanced selectivity toward CO_2 may arise from above 620 Torr following gate opening. We first measured single-gas breakthrough curves of CO_2 as a function of its partial pressure (Figure 5b). Mixtures of CO_2 and helium (as an inert carrier gas) were introduced to an adsorption column packed with 0.85 g of MUF-15-OMe. The total pressure was maintained at 1.1 bar and the temperature at 273 K. Feeds with four CO_2 partial pressures were introduced to the column (Table S5). The sharpness of the experimental breakthrough curves indicates that the adsorption rates are rapid. The first three partial pressures (412, 495, and 577 Torr) lie below the gate opening pressure. In these cases, the framework does not flex, and the progressively longer breakthrough times reflect the increased quantity of CO_2 (Figure 5b). At a CO_2 partial pressure of 783 Torr, on the other hand, MUF-15-OMe will be in its gate-opened form. Here, we observed a distinct jump in the breakthrough time since the structural transformation of MUF-15-OMe brings about a higher capacity for CO_2 uptake (Figure 5b). To further investigate this additional capacity, we simulated the CO_2 breakthrough curves.[27,43,44] Good agreement was observed between simulated and experimental breakthrough curves, confirming the validity of this model across feeds with different CO_2 concentrations (Figure 5b). Using this validated model, a breakthrough curve was then predicted for the feed mixture with a partial CO_2 pressure of 783 Torr under the hypothetical assumption that the framework structure remains static. This involved refitting the CO_2 adsorption isotherm below the gate opening pressure to obtain appropriate parameters (Figures 5c and S24). The breakthrough of CO_2 using this "inflexible" adsorbent is predicted to occur after 21 min, which is earlier than the simulation that allows for framework flexibility (23.3 min, Figure 5c). This demonstrates that gate opening enhances CO_2 capture under dynamic conditions.

To further demonstrate the effect of gate opening on binary gas mixtures where the two gases simultaneously adsorb, we investigated the separation of CO_2 and N_2. First, experimental breakthrough curves for a 60/40 CO_2/N_2 mixture (CO_2 partial pressure of 495 Torr) and an 85/15 CO_2/N_2 mixture (CO_2 partial pressure of 701 Torr) were measured (Figure S25). Simulated breakthrough curves show a good match with the experimental data (Figure S25). With this model in hand, we could compare the breakthrough separation of the 85/15 CO_2/N_2 mixture under two different scenarios: (i) that MUF-15-OMe is flexible and (ii) the hypothetical assumption that MUF-15-OMe is inflexible (Figures S23 and S24). When the flexibility of MUF-15-OMe is taken into account, the separation improves since the elution of CO_2 is delayed by more than 2 min (Figure 5d). On the other hand, the elution times for N_2 are very similar since it does not benefit from the additional pore space that is created by framework flexing. In this way, the structural transformation delivers an improved separation material.

In summary, MUF-15-OMe is a dynamic MOF that responds to guest uptake with a reversible, pore-expanding structural transformation. Adsorption in this newly created pore space is selective for particular guests, enabling good separations. Specifically, it improves the separation of CO_2 and N_2 and allows the quantum sieving of D_2 and H_2. The underlying mechanism behind the flexibility of MUF-15-OMe was deduced from computational studies, where one of the linkers partially detaches to allow the framework to expand and generate additional pore space. By illustrating how flexibility can enhance the uptake of specific guests, this study defines the way forward for challenging separations using dynamic MOFs.

■ ASSOCIATED CONTENT

Supporting Information

The Supporting Information is available free of charge at https://pubs.acs.org/doi/10.1021/acs.chemmater.1c03170.

TG curves, PXRD patterns, additional isotherm data, dual-site Langmuir−Freundlich isotherm model fitting, isosteric heat of adsorption calculation, BET surface area calculations, simulated and experimental breakthrough curves, calculation details, and additional isotope adsorption plots (PDF)

Crystallographic data for MUF-15-OMe (CCDC 2055679) (CIF)

Calculation files (ZIP)

■ AUTHOR INFORMATION

Corresponding Author

Shane G. Telfer − *MacDiarmid Institute for Advanced Materials and Nanotechnology, School of Fundamental Sciences, Massey University, Palmerston North 4410, New Zealand;* orcid.org/0000-0003-1596-6652; Email: s.telfer@massey.ac.nz

Authors

Omid T. Qazvini − *MacDiarmid Institute for Advanced Materials and Nanotechnology, School of Fundamental Sciences, Massey University, Palmerston North 4410, New Zealand; Department of Chemical Engineering and Analytical Science, University of Manchester, Manchester M13 9PL, U.K.;* orcid.org/0000-0002-7730-2440

Victoria-Jayne Scott − *MacDiarmid Institute for Advanced Materials and Nanotechnology, School of Fundamental Sciences, Massey University, Palmerston North 4410, New Zealand*
Linda Bondorf − *Max Planck Institute for Intelligent Systems, 70569 Stuttgart, Germany*
Maxime Ducamp − *Chimie ParisTech, PSL Research University, CNRS, Institut de Recherche de Chimie Paris, 75005 Paris, France*
Michael Hirscher − *Max Planck Institute for Intelligent Systems, 70569 Stuttgart, Germany;* orcid.org/0000-0002-3143-2119
François-Xavier Coudert − *Chimie ParisTech, PSL Research University, CNRS, Institut de Recherche de Chimie Paris, 75005 Paris, France;* orcid.org/0000-0001-5318-3910

Complete contact information is available at: https://pubs.acs.org/10.1021/acs.chemmater.1c03170

Notes

The authors declare no competing financial interest.

■ ACKNOWLEDGMENTS

The authors would like to thank Dr. Seok June (Subo) Lee and Dr. Prathapa Jagannatha (Bruker) for their assistance with X-ray crystallography. The authors gratefully acknowledge the MacDiarmid Institute and RSNZ Marsden Fund (Contract 14-MAU-024) for financial support. The authors acknowledge financial support from the Agence Nationale de la Recherche under project "MATAREB" (ANR-18-CE29-0009-01) and access to high-performance computing platforms provided by GENCI Grant A0090807069.

■ REFERENCES

(1) Furukawa, H.; Cordova, K. E.; O'Keeffe, M.; Yaghi, O. M. The Chemistry and Applications of Metal-Organic Frameworks. *Science* **2013**, *341*, No. 1230444.
(2) Kitagawa, S.; Kitaura, R.; Noro, S.-i. Functional Porous Coordination Polymers. *Angew. Chem., Int. Ed.* **2004**, *43*, 2334−2375.
(3) Qazvini, O. T.; Telfer, S. G. A Robust Metal−Organic Framework for Post-Combustion Carbon Dioxide Capture. *J. Mater. Chem. A* **2020**, *8*, 12028−12034.
(4) Qazvini, O. T.; Babarao, R.; Telfer, S. G. Selective Capture of Carbon Dioxide from Hydrocarbons Using a Metal-Organic Framework. *Nat. Commun.* **2021**, *12*, No. 197.
(5) Schneemann, A.; Bon, V.; Schwedler, I.; Senkovska, I.; Kaskel, S.; Fischer, R. A. Flexible Metal−Organic Frameworks. *Chem. Soc. Rev.* **2014**, *43*, 6062−6096.
(6) Krause, S.; Hosono, N.; Kitagawa, S. Chemistry of Soft Porous Crystals: Structural Dynamics and Gas Adsorption Properties. *Angew. Chem., Int. Ed.* **2020**, *59*, 15325−15341.
(7) Lin, Z.-J.; Lü, J.; Hong, M.; Cao, R. Metal−Organic Frameworks Based on Flexible Ligands (Fl-MOFs): Structures and Applications. *Chem. Soc. Rev.* **2014**, *43*, 5867−5895.
(8) Chang, Z.; Yang, D.-H.; Xu, J.; Hu, T.-L.; Bu, X.-H. Flexible Metal−Organic Frameworks: Recent Advances and Potential Applications. *Adv. Mater.* **2015**, *27*, 5432−5441.
(9) Zhang, J.-P.; Zhou, H.-L.; Zhou, D.-D.; Liao, P.-Q.; Chen, X.-M. Controlling Flexibility of Metal−Organic Frameworks. *Natl. Sci. Rev.* **2018**, *5*, 907−919.
(10) Horike, S.; Shimomura, S.; Kitagawa, S. Soft Porous Crystals. *Nat. Chem.* **2009**, *1*, 695−704.
(11) Zheng, J.-J.; Kusaka, S.; Matsuda, R.; Kitagawa, S.; Sakaki, S. Theoretical Insight into Gate-Opening Adsorption Mechanism and Sigmoidal Adsorption Isotherm into Porous Coordination Polymer. *J. Am. Chem. Soc.* **2018**, *140*, 13958−13969.
(12) Gu, C.; Hosono, N.; Zheng, J.-J.; Sato, Y.; Kusaka, S.; Sakaki, S.; Kitagawa, S. Design and Control of Gas Diffusion Process in a Nanoporous Soft Crystal. *Science* **2019**, *363*, 387−391.
(13) Xu, X.; Yang, F.; Chen, S.-L.; He, J.; Xu, Y.; Wei, W. Dynamic Behaviours of a Rationally Prepared Flexible Mof by Postsynthetic Modification of Ligand Struts. *Chem. Commun.* **2017**, *53*, 3220−3223.
(14) Hahm, H.; Yoo, K.; Ha, H.; Kim, M. Aromatic Substituent Effects on the Flexibility of Metal−Organic Frameworks. *Inorg. Chem.* **2016**, *55*, 7576−7581.
(15) Murdock, C. R.; Hughes, B. C.; Lu, Z.; Jenkins, D. M. Approaches for Synthesizing Breathing Mofs by Exploiting Dimensional Rigidity. *Coord. Chem. Rev.* **2014**, *258*−*259*, 119−136.
(16) Henke, S.; Schneemann, A.; Wütscher, A.; Fischer, R. A. Directing the Breathing Behavior of Pillared-Layered Metal−Organic Frameworks Via a Systematic Library of Functionalized Linkers Bearing Flexible Substituents. *J. Am. Chem. Soc.* **2012**, *134*, 9464−9474.
(17) Devic, T.; Horcajada, P.; Serre, C.; Salles, F.; Maurin, G.; Moulin, B.; Heurtaux, D.; Clet, G.; Vimont, A.; Grenèche, J.-M.; Ouay, B. L.; Moreau, F.; Magnier, E.; Filinchuk, Y.; Marrot, J.; Lavalley, J.-C.; Daturi, M.; Férey, G. Functionalization in Flexible Porous Solids: Effects on the Pore Opening and the Host−Guest Interactions. *J. Am. Chem. Soc.* **2010**, *132*, 1127−1136.
(18) Wannapaiboon, S.; Schneemann, A.; Hante, I.; Tu, M.; Epp, K.; Semrau, A. L.; Sternemann, C.; Paulus, M.; Baxter, S. J.; Kieslich, G.; Fischer, R. A. Control of Structural Flexibility of Layered-Pillared Metal-Organic Frameworks Anchored at Surfaces. *Nat. Commun.* **2019**, *10*, No. 346.
(19) Yang, L.; Cui, X.; Zhang, Y.; Yang, Q.; Xing, H. A Highly Sensitive Flexible Metal−Organic Framework Sets a New Benchmark for Separating Propyne from Propylene. *J. Mater. Chem. A* **2018**, *6*, 24452−24458.
(20) Wang, X.; Krishna, R.; Li, L.; Wang, B.; He, T.; Zhang, Y.-Z.; Li, J.-R.; Li, J. Guest-Dependent Pressure Induced Gate-Opening Effect Enables Effective Separation of Propene and Propane in a Flexible Mof. *Chem. Eng. J.* **2018**, *346*, 489−496.
(21) Li, L.; Krishna, R.; Wang, Y.; Yang, J.; Wang, X.; Li, J. Exploiting the Gate Opening Effect in a Flexible Mof for Selective Adsorption of Propyne from C1/C2/C3 Hydrocarbons. *J. Mater. Chem. A* **2016**, *4*, 751−755.
(22) Zeng, H.; Xie, M.; Huang, Y. L.; Zhao, Y.; Xie, X. J.; Bai, J. P.; Wan, M. Y.; Krishna, R.; Lu, W.; Li, D. Induced Fit of C_2H_2 in a Flexible MOF through Cooperative Action of Open Metal Sites. *Angew. Chem., Int. Ed.* **2019**, *58*, 8515−8519.
(23) Yu, M.-H.; Space, B.; Franz, D.; Zhou, W.; He, C.; Li, L.; Krishna, R.; Chang, Z.; Li, W.; Hu, T.-L.; et al. Enhanced Gas Uptake in a Microporous Metal−Organic Framework Via a Sorbate Induced-Fit Mechanism. *J. Am. Chem. Soc.* **2019**, *141*, 17703−17712.
(24) Suzuki, T.; Kotani, R.; Kondo, A.; Maeda, K. Structural Investigation of a Flexible MOF $[Cu(BF_4)_2(1,3\text{-Bis}(4\text{-pyridyl})\text{-propane})_2]$ Showing Selective Gate Adsorption with Dynamic Pore-Opening/Pore-Closing Processes. *J. Phys. Chem. C* **2016**, *120*, 21571−21579.
(25) Nijem, N.; Wu, H.; Canepa, P.; Marti, A.; Balkus, K. J.; Thonhauser, T.; Li, J.; Chabal, Y. J. Tuning the Gate Opening Pressure of Metal−Organic Frameworks (MOFs) for the Selective Separation of Hydrocarbons. *J. Am. Chem. Soc.* **2012**, *134*, 15201−15204.
(26) Carrington, E. J.; McAnally, C. A.; Fletcher, A. J.; Thompson, S. P.; Warren, M.; Brammer, L. Solvent-Switchable Continuous-Breathing Behaviour in a Diamondoid Metal−Organic Framework and Its Influence on CO_2 Versus CH_4 Selectivity. *Nat. Chem.* **2017**, *9*, 882−889.
(27) Qazvini, O. T.; Babarao, R.; Shi, Z.-L.; Zhang, Y.-B.; Telfer, S. G. A Robust Ethane-Trapping Metal−Organic Framework with a High Capacity for Ethylene Purification. *J. Am. Chem. Soc.* **2019**, *141*, 5014−5020.
(28) Qazvini, O. T.; Macreadie, L. K.; Telfer, S. G. Effect of Ligand Functionalization on the Separation of Small Hydrocarbons and CO_2 by a Series of MUF-15 Analogues. *Chem. Mater.* **2020**, *32*, 6744−6752.

(29) Dincă, M.; Dailly, A.; Liu, Y.; Brown, C. M.; Neumann, D. A.; Long, J. R. Hydrogen Storage in a Microporous Metal−Organic Framework with Exposed Mn^{2+} Coordination Sites. *J. Am. Chem. Soc.* **2006**, *128*, 16876−16883.
(30) Ortiz, A. U.; Boutin, A.; Coudert, F.-X. Prediction of Flexibility of Metal−Organic Frameworks CAU-13 and NOTT-300 by First Principles Molecular Simulations. *Chem. Commun.* **2014**, *50*, 5867−5870.
(31) Bousquet, D.; Coudert, F.-X.; Boutin, A. Free Energy Landscapes for the Thermodynamic Understanding of Adsorption-Induced Deformations and Structural Transitions in Porous Materials. *J. Chem. Phys.* **2012**, *137*, No. 044118.
(32) Kim, J. Y.; Zhang, L.; Balderas-Xicohténcatl, R.; Park, J.; Hirscher, M.; Moon, H. R.; Oh, H. Selective Hydrogen Isotope Separation Via Breathing Transition in MIL-53 (Al). *J. Am. Chem. Soc.* **2017**, *139*, 17743−17746.
(33) Choi, H. J.; Dinca, M.; Long, J. R. Broadly Hysteretic H_2 Adsorption in the Microporous Metal− Organic Framework Co (1, 4-Benzenedipyrazolate). *J. Am. Chem. Soc.* **2008**, *130*, 7848−7850.
(34) Niimura, S.; Fujimori, T.; Minami, D.; Hattori, Y.; Abrams, L.; Corbin, D.; Hata, K.; Kaneko, K. Dynamic Quantum Molecular Sieving Separation of D_2 from H_2−D_2 Mixture with Nanoporous Materials. *J. Am. Chem. Soc.* **2012**, *134*, 18483−18486.
(35) Oh, H.; Hirscher, M. Quantum Sieving for Separation of Hydrogen Isotopes Using MOFs. *Eur. J. Inorg. Chem.* **2016**, *2016*, 4278−4289.
(36) Cao, D.; Huang, H.; Lan, Y.; Chen, X.; Yang, Q.; Liu, D.; Gong, Y.; Xiao, C.; Zhong, C.; Peng, S. Ultrahigh Effective H_2/D_2 Separation in an Ultramicroporous Metal−Organic Framework Material through Quantum Sieving. *J. Mater. Chem. A* **2018**, *6*, 19954−19959.
(37) Oh, H.; Savchenko, I.; Mavrandonakis, A.; Heine, T.; Hirscher, M. Highly Effective Hydrogen Isotope Separation in Nanoporous Metal−Organic Frameworks with Open Metal Sites: Direct Measurement and Theoretical Analysis. *ACS Nano* **2014**, *8*, 761−770.
(38) Zhang, L.; Jee, S.; Park, J.; Jung, M.; Wallacher, D.; Franz, A.; Lee, W.; Yoon, M.; Choi, K.; Hirscher, M.; et al. Exploiting Dynamic Opening of Apertures in a Partially Fluorinated MOF for Enhancing H_2 Desorption Temperature and Isotope Separation. *J. Am. Chem. Soc.* **2019**, *141*, 19850−19858.
(39) von Zeppelin, F.; Haluška, M.; Hirscher, M. Thermal Desorption Spectroscopy as a Quantitative Tool to Determine the Hydrogen Content in Solids. *Thermochim. Acta* **2003**, *404*, 251−258.
(40) Van Assche, T. R. C.; Baron, G. V.; Denayer, J. F. M. Molecular Separations with Breathing Metal−Organic Frameworks: Modelling Packed Bed Adsorbers. *Dalton Trans.* **2016**, *45*, 4416−4430.
(41) Hamon, L.; Llewellyn, P. L.; Devic, T.; Ghoufi, A.; Clet, G.; Guillerm, V.; Pirngruber, G. D.; Maurin, G.; Serre, C.; Driver, G.; van Beek, W.; Jolimaître, E.; Vimont, A.; Daturi, M.; Férey, G. Co-Adsorption and Separation of CO_2−CH_4 Mixtures in the Highly Flexible MIL-53(Cr) MOF. *J. Am. Chem. Soc.* **2009**, *131*, 17490−17499.
(42) Remy, T.; Baron, G. V.; Denayer, J. F. M. Modeling the Effect of Structural Changes During Dynamic Separation Processes on MOFs. *Langmuir* **2011**, *27*, 13064−13071.
(43) Qazvini, O. T.; Babarao, R.; Telfer, S. G. Multipurpose Metal−Organic Framework for the Adsorption of Acetylene: Ethylene Purification and Carbon Dioxide Removal. *Chem. Mater.* **2019**, *31*, 4919−4926.
(44) Qazvini, O. T.; Fatemi, S. Modeling and Simulation Pressure−Temperature Swing Adsorption Process to Remove Mercaptan from Humid Natural Gas; a Commercial Case Study. *Sep. Purif. Technol.* **2015**, *139*, 88−103.

https://doi.org/10.1021/acs.chemmater.1c03170
Chem. Mater. 2021, 33, 8886−8894